Proceedings of the Korean Nuclear Society Spring Meeting

Gyeongju, Korea, 2004

Development of a Modified Reconstruction Algorithm for 90-Degree Compton Scattering Imaging

Sang Hoon Lee[*], Tran Kim Tuan[**], Sung Ho Park[***] and Jong Kyung Kim[**]

[*]Innovative Technology Center for Radiation Safety (iTRS) and
[**]Department of Nuclear Engineering, Hanyang University
17 Haengdang, Sungdong, Seoul, Korea 133-791

[***]Hallym University Sacred Heart Hospital
Anyang, Kyunggi, Korea 431-070

ABSTRACT

A modified reconstruction algorithm has been developed for an X-ray luggage inspection modality based on 90˚ Compton scattering imaging. Incident photon energy E_0 of 122.1keV was used in simulated experiments with MCNP for 5x5x5 samples and the 90˚ Compton scattered photon energy E_1 is 98.6keV. In the $\mu_t(E_1)$ reconstruction calculation the least-squares solution was computed through Householder transformations applied in blocked form for the full $\mu_t(E_1)$ over-determined system equations of the side detector responses in the simulated experiments. In the $\mu_t(E_0)$ $\mu_c(E_0)$ reconstruction calculation, instead of $\mu_t(E_0) = \mu_c(E_0)$ approximation which does not hold true for the source energy of this paper, the semi-empirical formula $\mu_t(E_0) = d^*\mu_c(E_0)+e^* \mu_t(E_1)$ was used and the least-squares solution was computed with the conjugate gradient method for $\mu_t(E_0)$ $\mu_c(E_0)$ system equations of the side and transmission detector responses and the semi-empirical formulae. Self attenuation correction factors in a simple form were applied in an iterative manner until the factors and reconstruction output are converged. The maximum errors of the reconstruction calculation for a sample with aluminum core and polyethylene matrix were –2.9% for $\mu_t(E_0)$, -1.0% for $\mu_t(E_1)$, and 1.9% for $\mu_c(E_0)$, showing good agreements with theoretical values. The maximum errors for the case with steel core and polyethylene matrix were –10.2% for $\mu_t(E_0)$, -3.3% for $\mu_t(E_1)$, and 20.3% for $\mu_c(E_0)$, indicating that this case with 3 cm steel rod would be a limiting case for the penetration ability of 122.1keV incident photons used in the inspection modality.

1. Introduction

Since the tragic collapse of World Trade Center in New York on September 11, 2001 caused by two hijacked airplanes security concerns on all aspects have been much intensified than before. Many already developed systems of security inspection, including typical X-ray luggage scans, have been widely adapted at many ports and security check points. New inspection modalities based on new

technologies are on high demand to make up for some weak points in the currently available inspection systems, for example, lack of detailed material information other than attenuation in typical X-ray luggage scans.

One of the new modalities, based on X-ray Compton scattering imaging, is under development [1,2,4]. Inspection system based on X-ray Compton scattering imaging does not require costly rotation system as in conventional CT system. And with more theoretical development in the future there are possibilities of local material identification. Our research group developed a reconstruction algorithm for 661keV source photon [4] and has focused on a modified reconstruction algorithm for 122keV source photons in this paper.

With the adoption of high energy x-rays like 662keV source, the reconstruction can be done easily with the help of the assumption of $\mu_t(E_0) = \mu_c(E_0)$ but, on the other side, the reconstruction output, $\mu_t(E_0)$, $\mu_c(E_0)$ *and* $\mu_t(E_1)$ all are closely related to each other and in essence only material density is revealed because in this energy range Compton scattering is the dominant reaction of all. With the adoption of lower energy x-rays like 122keV source, more information is included in the reconstruction output since in this energy range Compton scattering and photoelectric absorption are competing with each other and there are possibilities of identifying the material.

Since the assumption $\mu_t(E_0) = \mu_c(E_0)$ does not hold true any more for lowered energy sources like 122keV photons, a new semi-empirical formula $\mu_t(E_0) = d^*\mu_c(E_0)+e^* \mu_t(E_1)$ has been developed and used in the reconstruction algorithm. And also for the increased self-attenuations in reacting volumes more complex self attenuation correction models than simple half-thickness model has been developed for incoming photons from the source and outgoing photons to the side detectors. MCNP simulated experiments were performed to provide detector responses to the reconstruction algorithm. The final reconstruction output $\mu_t(E_0)$, $\mu_c(E_0)$ *and* $\mu_t(E_1)$ were compared with theoretical values.

2. Materials and Method

2.1 Compton Scattering Imaging System

A usual Compton scattering imaging system is made up with a collimated photon source, a transmission detector and four side detectors. For each node or voxel in a sample, five detector responses (one transmission and four sides) are obtained from experiments or simulated experiments as in this paper. The detector responses are post-processed in a reconstruction program to provide material information of each node, which are $\mu_t(E_0)$, $\mu_c(E_0)$ *and* $\mu_t(E_1)$, or in other notations μ, μ_c *and* μ'.

In the 90˚ Compton scattering system a sample or an object can be considered as NX×NY×NZ voxels, where NX, NY, and NZ are the number of voxels along the direction of X, Y, and Z, respectively, as shown in Fig.1. When a beam of gamma rays is incident on the object, the intensities of the transmission and scattering radiations at the angle of 90˚ are measured at the same time by a transmission detector (Tr) and 4 scattering detector arrays which are indicated conveniently as top (T), bottom (B), left (L) and right (R). The incident beam is moved in a plane parallel with the cross section of the object, from left to right and from top to bottom with steps equal to the size of a voxel until the entire one side of the object is exposed. For simplification, the attenuation effects of gamma rays in the air before coming into the object and after going out from the object to the detector are neglected. Assuming the scattering is occurred at the center of the voxel (i, j, k), where (i, j, k) indicates the voxel located at i-th, j-th and k-th along the direction of X, Y, and Z, respectively, the single scattered response of a left detector $L_{i,j,k}$ can be expressed as [1,2]

$$L_{ijk} = L^0_{ijk}\mu_{C,ijk} \exp\left\{-\Delta x^{in} \sum_{m=NX-1}^{i+1} \mu_{mjk} - \frac{1}{2}\Delta x^{in}\mu_{ijk} - \Delta x^{out} \sum_{m=0}^{j-1} \mu'_{imk} - \frac{1}{2}\Delta x^{out}\mu'_{ijk}\right\} \quad (1)$$

where $\mu_{i,j,k}$ and $\mu'_{i,j,k}$ (or, $\mu_t(E_0)$ and $\mu_t(E_1)$) are the total linear attenuation coefficients of the voxel (i,j,k)

at the incident and the scattering energies and $\mu_{C,i,j,k}$ is the Compton scattering attenuation $\mu_c(E_0)$ of the voxel. Δx^{in} and Δx^{out} are the sizes of the voxel corresponding to the direction of the incident and scattering pathway, respectively. L^0 is a system constant depending the source intensity, the detector efficiency and the system geometry. Similar expressions can be written for the responses of right, top and bottom detectors. The response of the transmission detector can be written in the similar form as follows

$$Tr_{jk} = Tr_{jk}^{0} \exp\left(-\Delta x^{in} \sum_{m=0}^{NX-1} \mu_{mjk}\right) \quad (2)$$

The attenuation coefficients are considered as unknowns, hence there are three unknowns in Eq.(1) and 3×NX×NY×NZ unknowns for the whole object. The image reconstruction problem is an inverse problem in which three unknowns $\mu_t(E_0)$, $\mu_t(E_1)$ and $\mu_c(E_0)$ in Eq.(1) for individual voxels are solved from 4×NX×NY×NZ scattering detector measurements and NY×NZ transmission detector measurements. These unknowns are physically related but they can be independently calculated in different process. Based on the fact that all scattering measurements to a particular voxel have the same pre-scattering attenuation and the ratio of any two scattering measurements provides an estimate of the post-scattering attenuation, therefore $\mu_t(E_1)$ can be directly obtained from ratios of any pair of scattering measurements using linear algebraic method for an over-determined system. Knowing $\mu_t(E_1)$, Eq.(1) becomes an equation of two variables $\mu_t(E_0)$ and $\mu_c(E_0)$ which can be solved by using a nonlinear iterative process with the transmission response provided by Eq.(2). For getting minimized error propagation and the best quality of the images, the least squares method is applied in the reconstruction process.

2.2 Simulated Experiments with MCNP

In order to obtain radiation responses of detectors without experiment measurements for demonstrating the reconstruction algorithm, a small object is used in MCNP simulation. The object consists of 5×5×5 voxels, each voxel is a 1×1×1cm cube. Core materials with the size of 3×1×1 voxels are located in the center of the object and the other surrounding voxels are made up with a background material. The values in Table 1 are the attenuation coefficients at energy of 122keV to illustrate an object consisting of aluminum core and polyethylene background.

The materials used in the simulation are common materials with density in the range of common luggage from 0.94g/cm^3 of polyethylene up to 8.5g/cm^3 of brass. To examine the performance of the suggested algorithm for the ideal cases, well-collimated detectors and unique relationship between the incident and scattering energies are adopted and only single scattering gamma rays are assumed to record a count in detectors. The gamma source used in this simulation is Co-59 isotope source and, for simplification, the gamma beam is assumed to be a parallel pencil beam. The detectors used in the simulation are point detectors with tally 5 options.

2.3 Modified Reconstruction Algorithm

The reconstruction process combines two steps; (1) directly calculation of $\mu_t(E_1)$ using linear matrix inversion and (2) the nonlinear iterative reconstruction for $\mu_t(E_0)$ and $\mu_c(E_0)$. Self attenuation corrections are involved in both steps.

2.3.1 $\mu_t(E_1)$ Calculation

Each scattering response corresponding to a particular voxel (i,j,k) contains the same pre-scattering attenuation, hence a ratio of any two scattering measurements is an equation of $\mu_t(E_1)$ only. For example, for a voxel (i,j,k) on a plane containing four side detectors, the following equations can be written:

$$\log(L_{ijk}) - \log(B_{ijk}) = -\sum_{m=0}^{j-1} \mu'_{imk}\Delta + \sum_{m=0}^{k-1} \mu'_{ijm}\Delta$$
$$\log(R_{ijk}) - \log(B_{ijk}) = -\sum_{m=j+1}^{NY-1} \mu'_{imk}\Delta + \sum_{m=0}^{k-1} \mu'_{ijm}\Delta \quad (3)$$
$$\log(T_{ijk}) - \log(B_{ijk}) = -\sum_{m=k+1}^{NZ-1} \mu'_{ijm}\Delta + \sum_{m=0}^{k-1} \mu'_{ijm}\Delta$$

where, for simplification, let assume $\Delta x^{in} = \Delta x^{out} = \Delta$.

For the plane holding NY×NZ voxels, the number of equations is NY×NZ×3-4 which is larger then the number of unknowns NY×NZ. In a matrix notation, Eq.(3) can be written as follows for the slice of voxels on the plane.

$$\mathbf{R = A.\mu'_t} \quad (4)$$

This over-determined system equations can be easily solved by using linear matrix inversion method. To obtain $\mu_t(E_1)$ images of whole object the reconstruction process for $\mu_t(E_1)$ is repeated for all slices.

2.3.2 $\mu_t(E_0)$ and $\mu_c(E_0)$ Calculation

With known $\mu_t(E_1)$, Eq.(1) becomes a nonlinear equation with two unknowns $\mu_t(E_0)$ and $\mu_c(E_0)$. In order to solve this equation more one needs some more information on the two variables. An iteration process with a correction factor calculated from transmission measurements can be used in finding the reliable value of $\mu_t(E_0)$ and $\mu_c(E_0)$ by assuming $\mu_t(E_0) \approx \mu_c(E_0)$ [3,4]. This reconstruction process works well in the gamma energy range from a few hundreds keV to ~1MeV where Compton scattering dominates the photoelectric absorption. From Fig.(2) of the attenuation coefficients at 662keV-energy, the assumption is probable for most elements with atomic number Z less than 70. However, the assumption is not suitable in lower gamma energy range or for a medium which has high atomic number Z. In these cases the photoelectric absorption portion in the total attenuation coefficient is considerably large so that the assumption causes high errors in the inversion reconstruction problem.

To avoid the assumption, a method for estimating $\mu_t(E_0)$ that can be applied for iteration reconstruction processes with any incident gamma energy is introduced. A semi-empirical formula for total attenuation coefficient at the incident energy is built. In the geometry of 90˚ Compton scattering of gamma rays, the total attenuation coefficient can be expressed in the following formula

$$\mu_t = \mu_{pe} + \mu_C = \left(\sigma_{pe} + Z\sigma_C\right)\rho\frac{N_A}{A} \quad (5)$$

where μ_{pe} is the photoelectron absorption of the gamma ray in a medium with the atomic number Z and mass number A. Eq.(8) is rearranged as follows

$$\mu_t = a + b\mu_C \quad (6)$$

where a and b are coefficients considered as constant with an incident energy of gamma rays. The post-scattering energy E_1 is uniquely related to the incident energy E_0 by the well-known equation

$$E_1 = \frac{E_0}{1 + \frac{E_0}{m_0 c^2}\left(1 - \cos\theta\right)} \quad (7)$$

Therefore the relation between $\mu_t(E_0)$ and $\mu_t(E_1)$, $\mu_c(E_0)$ can be suggested in a semi-empirical linear function as follows

$$\mu_t\left(E_0\right) = d * \mu_t\left(E_1\right) + e * \mu_C\left(E_0\right) \quad (8)$$

where d and e are constant coefficients which are dependent on the gamma energy only. With the semi-empirical equation and known $\mu_t(E_1)$, Eq.(1) can be solved to provide the reconstructed images of the

object for $\mu_t(E_0)$ and $\mu_c(E_0)$.

2.3.3 Self Attenuation Correction

In order to have the reconstructed images closer to the true images, the self attenuation effects should be considered. In the previous governing equations for 90˚ Compton scattering effects, the scattering is assumed happening at the center of the voxel. The assumption may cause the big relative errors of the inverse problem because actually the scattering can occur anywhere in the voxel volume and depart to a scattering detector, hence a correction factor is introduced to evaluate this effect. The correction factor for the self attenuation is defined as

$$\alpha = \alpha_{in}\alpha_{out} = \frac{P'_{in}}{P_{in}}\frac{P'_{out}}{P_{out}} \tag{9}$$

where P_{in} and P_{out} are the attenuation factors of in-coming and out-going gamma rays for the voxel, respectively. P_{in} and P_{out} are calculated by assuming that all gamma rays scatter at the center of the voxel, and the primed ones are calculated by the following algebra equations assuming the scattering occurs in the whole voxel. With the assumption that the scattering occurs in the center of the voxel, the attenuations for pre- and post-scattering in the voxel are given by

$$P_{in} = \exp(-\mu_{ijk}\frac{\Delta}{2}) \qquad P_{out} = \exp(-\mu'_{ijk}\frac{\Delta}{2}) \tag{10}$$

Considering the fact that scattering occurs in the whole voxel volume, the attenuations can be obtained as

$$\begin{aligned} P'_{in} &= \frac{1}{\mu_{ijk}\Delta}\left[1-\exp(-\mu_{ijk}\frac{\Delta}{2})\right] \\ P'_{out} &= \frac{1}{\mu'_{ijk}\Delta}\left[1-\exp(-\mu'_{ijk}\frac{\Delta}{2})\right] \end{aligned} \tag{11}$$

A reconstruction algorithm for getting the images for $\mu_t(E_0)$, $\mu_t(E_1)$ and $\mu_c(E_0)$ is suggested as shown in Fig.3. In the iteration process of the flowchart the correction factors in Eq.(9) are used for re-evaluating the detector responses. The semi-empirical function Eq.(8) is used for solving the nonlinear equation in the iteration calculation.

3. Results

In Fig. 4 are shown the total attenuation coefficients from XCOM version 3.1 data for gamma energies at 662keV and 122keV and the semi-empirical approximations for them. The fitted curves have good agreements with the XCOM photon data. The relative errors in comparison between the true value and the approximation are less than 5% in the case of 662keV. With E_0 = 122keV the errors are less than 6% for all elements except for the elements with the atomic numbers from Z=87 to Z=94. This results show that the approximation for $\mu_t(E_0)$ by using the semi-empirical function Eq.(8) fits well to the true value of $\mu_t(E_0)$ and looks reasonably goof for reconstruction iteration processes.

Table 2 shows some results of the old reconstruction algorithm using the detector responses from the MCNP simulations with the assumption of $\mu_t(E_0) \approx \mu_c(E_0)$ and without correction factors for self attenuation effects. The errors of $\mu_t(E_1)$ reconstruction (Table 2.c) are low for most elements that have not only low atomic number but also high atomic number. For example they are less than 1% with polyethylene that has Z_{eff} = 5.28 and about 3.3% for steel (Z_{eff} = 25.61). The reconstruction problem for $\mu_t(E_1)$ is a direct inversion of a linear algebraic system shown in Eq.(4). The errors of $\mu_t(E_0)$ and $\mu_c(E_0)$ (Table 2.a for $\mu_t(E_0)$, Table 2.b and 2.d for $\mu_c(E_0)$) are much higher then those of $\mu_t(E_1)$. They are about 2% for low atomic number as polyethylene, from 10% to 20% for aluminium and are very high with high atomic number materials like steel. Therefore a modification for the reconstruction algorithm is needed for getting better images.

Modifications suggested in the work are the use of the semi-empirical function for the evaluation of $\mu_t(E_0)$ in the iteration process and the correction factors for the self attenuation effects. The results of the new reconstruction algorithm are in better agreements with theoretical values as shown in Table 3. For $\mu_t(E_1)$ (Table 3.c and 3.e) the improvements in errors are not big, though the new results are much closer to the true values because $\mu_t(E_1)$ is now evaluated directly from detector responses with a linear equation system. The $\mu_t(E_1)$ errors are 0.8% for polyethylene, 2.9% for aluminium and 3.3% for steel and theses are quite good results for luggage inspection purposes. The invert results for $\mu_t(E_0)$ and $\mu_c(E_0)$ obtained by using the suggested new reconstruction algorithm are in good agreements with the theoretical values. From Table 3.a and 3.d, the $\mu_t(E_0)$ errors are 0.8%, 1.0% and 10.2% for polyethylene, aluminium and steel, respectively, in comparison with 0.9% (PE) and 18.6% (aluminium) from Table 2.a. The improvements in errors are larger in the reconstructed values of $\mu_c(E_0)$, from 1.8%, 7.2% and 1630% (Table 2.b and 2.d) to 1.6%, 1.9% and 20.3% (Table 3.c and 3.f) for polyethylene, aluminium and steel, respectively. Since the results from the newly suggested reconstruction algorithm show good accuracy, it can be concluded that the iteration method with the semi-empirical function and the correction factors for the self attenuation effects performs well and is able to reconstruct images in the 90° Compton scattering inspection system.

4. Conclusions and Discussions

The modified new reconstruction algorithm showed better agreements with true values than the original algorithm. The main reason for the better agreements is that the semi-empirical formula is more accurate than rough approximation $\mu_t(E_0) = \mu_c(E_0)$ in the energy range of this paper. Also improvements come from that the modified algorithm takes full use of all system equations in the $\mu_t(E_1)$ calculation and that the correction factors better than the original simple approximation of half-thickness attenuation are introduced to model the effects of self attenuation in the cell of interest.

By using complete full matrix form of system equation in the calculations of $\mu_t(E_1)$ and $\mu_t(E_0)$ $\mu_c(E_0)$ the algorithm became simpler, cleaner and mathematically more clearly refined than before. The concern that comes from the program modification is for cases with many cells, which will inevitably increase the matrix size and burden the least-squares routines for over-determined systems. But the burden is not much because $\mu_t(E_1)$ and $\mu_t(E_0)$ $\mu_c(E_0)$ calculations are completely separated and $\mu_t(E_1)$ calculation only deals with 2-dimensional NY×NZ unknowns, and $\mu_t(E_0)$ $\mu_c(E_0)$ calculation only deals with 1-dimensional 2×NX unknowns.

With the newly modified reconstruction algorithm it has became possible to obtain three pieces of cell information, $\mu_t(E_1)$ $\mu_t(E_0)$ $\mu_c(E_0)$, at the photon energy of 122keV or around it with reasonable errors. These three cross section data can be used in identifying the material of the voxel, at least in finding effective-Z and density. But there are some expected limits on material identification. The expected limits are that in the energy range of around 122keV, Compton scattering is still dominant over the other reactions and the most important information in identifying material, the photoelectric absorption cross section is small for most elements except some heavy elements and because of that it is hard to identify all the materials. But it is expected that effective-Z and density can be obtained from three pieces of reconstruction information of the voxel.

In the near future, the modified reconstruction calculations will be performed for measured detector responses. Experimental data adopting 122keV source and CsI scattering detectors and YAP transmission detectors will be available in a few months, while the case with 450KV X-ray tube source will require more time. After that material identification routines will be developed for real application of the inspection system.

Acknowledgement

This work has been funded by the long-term nuclear research and development program of Ministry of Science and Technology of Korea, and by the Innovative Technology Center for Radiation Safety (iTRS) of Hanyang University sponsored by Korea Science and Engineering Foundation.

References

1. Arendtsz, N.V., Hussein, E.M.A., “Energy-Spectral Compton Scatter Imaging – Part I: Theory and Mathematics,” *IEEE Trans. Nucl. Sci,* **42 (6)** 2155-2165 (1995)
2. Arendtsz, N.V., Hussein E.M.A., “Energy-Spectral Compton Scatter Imaging – Part II: Experiments,” *IEEE Trans. Nucl. Sci.*, **42 (6)** 2166-1272 (1995)
3. Cesareo, R., Balogun, F., Brunetti, A., Borlino C.C., “90^{O} Compton and Rayleigh Measurements and Imaging,” *Radiation Phys. Chem.,* **61** 339-342 (2001)
4. T.K. Tuan, S.H. Park, and J.K. Kim, “Development of a New Reconstruction Algorithm for Compton Scattering Imaging,” *in Proc. ISORD-2*, Sendai, Japan, July 24-25, 2003
5. J.S. Park, S.H. Park, and J.K. Kim, “A Transmission Experiment using YAP and CsI to develop a X-ray inspection System,” *in Proc. Spring meeting of Korean Association for Radiation Protection*, Seoul, April 26, 2003
6. XCOM: Photon Cross Sections Database, Version 3.1.
7. Battista, J.J., Santon, L. W., Bronskill, M.J.”Compton scatter imaging of transverse sections: Corrections for multiple scatter and attenuations.” *Physics in Medicine and Biology* 22 (2), 229-244 (1977)
8. Evans, R.D. The Atomic Nucleus. *Robert E. Krieger Publishing Company*, Malabar, Florida (1982)

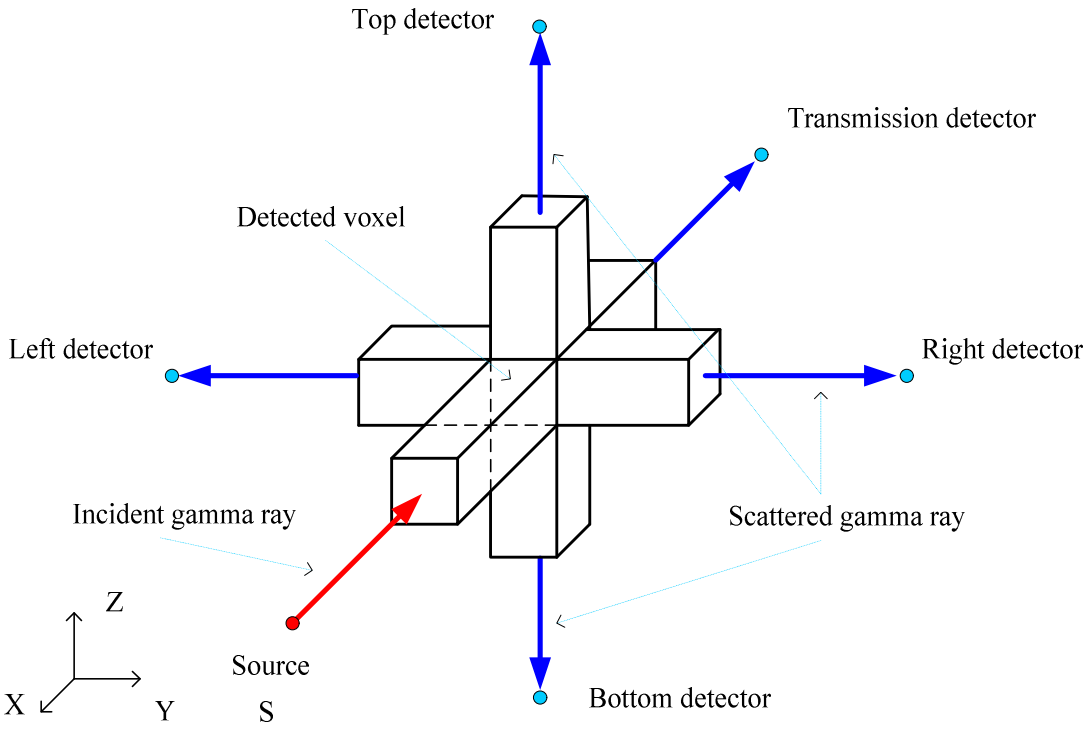

Fig.1 Geometry of 90° Compton scattering system

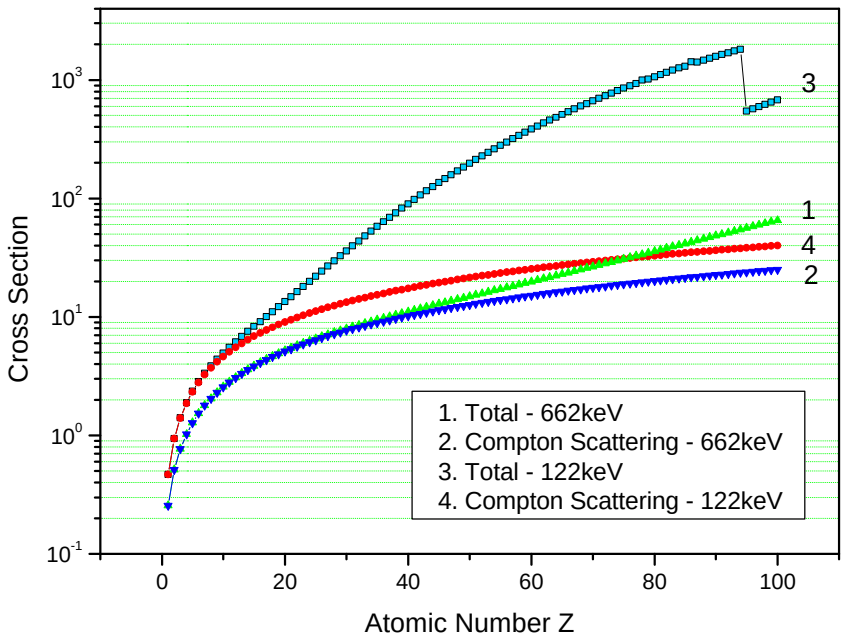

Fig.2 Photon Cross Sections

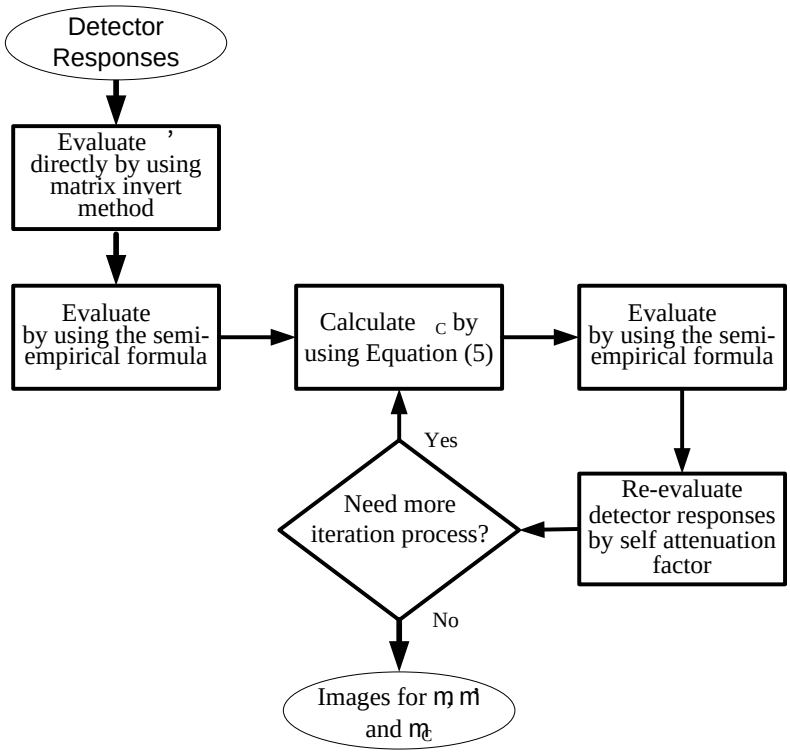

Fig.3 The flowchart of the iteration process for inverse problem

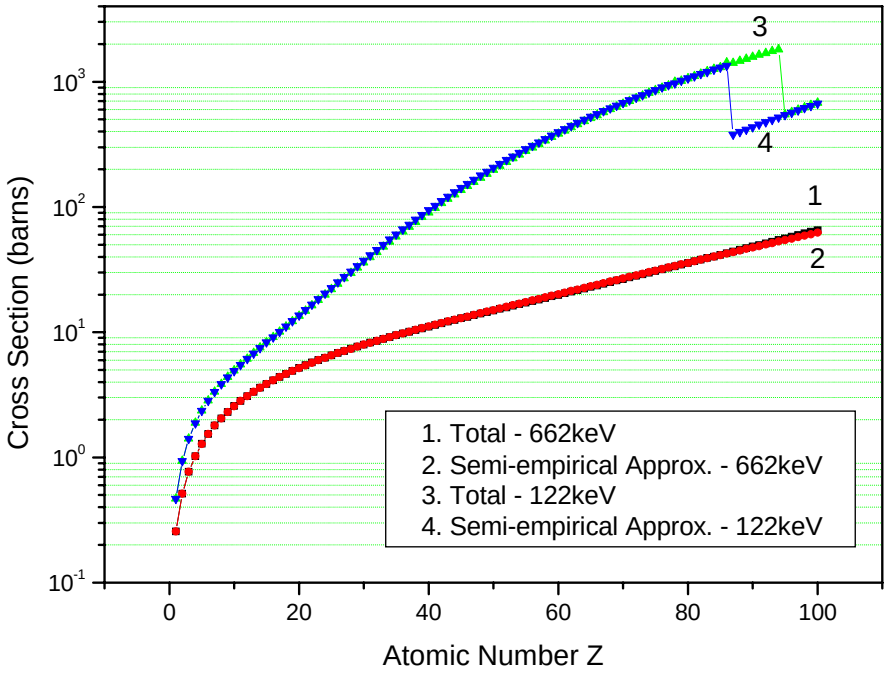

Fig. 4 Total cross section and the semi-empirical approximation as functions of atomic number Z

Table 1: 122keV attenuation coefficient map of the sample with aluminum core and polyethylene background (at i-j plane with k=2, bold typing indicates core material)

a) Total attenuation coefficient (cm^{-1})

	j=0	j=1	j=2	j=3	j=4
i=0	0.152	0.152	0.152	0.152	0.152
i=1	0.152	0.152	***0.421***	0.152	0.152
i=2	0.152	0.152	***0.421***	0.152	0.152
i=3	0.152	0.152	***0.421***	0.152	0.152
i=4	0.152	0.152	0.152	0.152	0.152

b) Compton attenuation coefficient (cm^{-1})

	j=0	j=1	j=2	j=3	j=4
i=0	0.149	0.149	0.149	0.149	0.149
i=1	0.149	0.149	***0.36***	0.149	0.149
i=2	0.149	0.149	***0.36***	0.149	0.149
i=3	0.149	0.149	***0.36***	0.149	0.149
i=4	0.149	0.149	0.149	0.149	0.149

Table 2: The related errors (%) of attenuation coefficients obtained from the imaging reconstruction algorithm using the assumption $\mu_t(E_0) \approx \mu_c(E_0)$

a) $\mu_t(E_0)$ errors for the sample with aluminum core and polyethylene background

	j=0	j=1	j=2	j=3	j=4
i=0	-0.9	-0.9	-6.3	-0.9	-0.9
i=1	-0.4	-0.4	***-12.2***	-0.4	-0.4
i=2	-0.5	-0.5	***-4.3***	-0.5	-0.5
i=3	0.5	0.5	***1.6***	0.5	0.5
i=4	0.5	0.5	18.4	0.5	0.5

b) $\mu_c(E_0)$ errors for the sample with aluminum core and polyethylene background

	j=0	j=1	j=2	j=3	j=4
i=0	0.7	0.7	1.1	0.7	0.7
i=1	1.0	1.0	***4.5***	1.0	1.0
i=2	0.8	0.8	***7.2***	0.9	0.8
i=3	1.8	1.8	***6.6***	1.7	1.8
i=4	1.7	1.7	3.1	1.7	1.7

c) $\mu_t(E_1)$ errors for the sample with steel core and polyethylene background

	j=0	j=1	j=2	j=3	j=4
i=0	0.7	0.6	0.7	0.8	0.7
i=1	0.7	0.9	***-3.3***	0.8	0.8
i=2	0.8	0.7	***-3.3***	0.7	0.7
i=3	0.8	0.8	***-3.3***	0.6	0.9
i=4	0.7	0.8	0.7	0.8	0.8

d) $\mu_c(E_0)$ errors for the sample with steel core and polyethylene background

	j=0	j=1	j=2	j=3	j=4
i=0	0.7	0.7	8.2	0.7	0.7
i=1	1.0	1.1	***269.7***	1.0	1.0
i=2	0.8	0.8	***1630.1***	0.8	0.8
i=3	1.8	1.8	***888.3***	1.7	1.8
i=4	1.7	1.7	61.3	1.7	1.7

Table 3: The related error (%) of attenuation coefficients obtained from the imaging reconstruction using the semi-empirical approximation and the self-attenuation correction factors

a) $\mu_t(E_0)$ errors for the sample with aluminum core and polyethylene background

	j=0	j=1	j=2	j=3	j=4
I=0	0.7	0.7	0.7	0.8	0.7
I=1	0.7	0.8	***-1.0***	0.7	0.7
I=2	0.8	0.7	***-1.0***	0.8	0.7
I=3	0.7	0.8	***-1.0***	0.7	0.8
I=4	0.7	0.8	0.7	0.8	0.7

b) $\mu_t(E_1)$ errors for the sample with aluminum core and polyethylene background

	j=0	j=1	j=2	j=3	j=4
i=0	0.1	0.1	0.3	0.1	0.1
i=1	0.1	0.1	***-2.9***	0.1	0.1
i=2	0.1	0.1	***-2.9***	0.1	0.1
i=3	0.3	0.3	***-2.9***	0.3	0.3
i=4	0.3	0.3	0.2	0.3	0.3

c) $\mu_c(E_0)$ errors for the sample with aluminum core and polyethylene background

	j=0	j=1	j=2	j=3	j=4
i=0	0.7	0.8	1.6	0.8	0.8
i=1	1.0	1.0	***1.7***	1.0	1.0
i=2	0.7	0.7	***1.9***	0.7	0.7
i=3	1.5	1.5	***1.9***	1.5	1.6
i=4	1.5	1.5	1.4	1.5	1.5

d) $\mu_t(E_0)$ errors for the sample with steel core and polyethylene background

	j=0	j=1	j=2	j=3	j=4
i=0	0.1	-0.1	6.4	0.1	0.1
i=1	0.1	0.1	***-6.4***	0.1	0.1
i=2	0.1	-0.1	***-8.9***	-0.1	0.1
i=3	0.3	0.3	***-10.2***	0.2	0.3
i=4	0.3	0.3	-2.5	0.3	0.3

e) $\mu_t(E_1)$ errors for the sample with steel core and polyethylene background

	j=0	j=1	j=2	j=3	j=4
i=0	0.7	0.7	0.7	0.8	0.7
i=1	0.7	0.7	***-3.3***	0.8	0.8
i=2	0.7	0.7	***-3.3***	0.7	0.7
i=3	0.8	0.7	***-3.3***	0.8	0.8
i=4	0.7	0.8	0.7	0.8	0.7

f) $\mu_c(E_0)$ errors for the sample with steel core and polyethylene background

	j=0	j=1	j=2	j=3	j=4
i=0	0.8	0.7	8.7	0.7	0.8
i=1	1.0	0.9	***20.3***	0.9	1.0
i=2	0.7	0.7	***5.6***	0.7	0.7
i=3	1.5	1.5	***-1.9***	1.5	1.6
i=4	1.5	1.5	-0.8	1.5	1.5